RSC Advances

PAPER

View Article Online
View Journal | View Issue

Cite this: *RSC Adv.*, 2022, **12**, 17237

Co-catalysis of trace dissolved Fe(III) with biochar in hydrogen peroxide activation for enhanced oxidation of pollutants†

Dongqing Feng,[a] Jianxin Shou,*[b] Sen Guo,[a] Mengna Ya,[a] Jianfa Li,*[a] Huaping Dong[a] and Yimin Li[a]

Activation of hydrogen peroxide (H_2O_2) with biochar is a sustainable and low-cost approach for advanced oxidation of organic pollutants, but faces the challenge of a low yield of hydroxyl radical (˙OH). Herein, we hypothesize that the activation efficiency of H_2O_2 can be enhanced through co-catalysis of trace dissolved iron (Fe) with biochar. Two biochar samples derived from different feedstock, namely LB from liquor-making residue and WB from wood sawdust, were tested in the co-catalytic systems using trace Fe(III) (0.3 mg L^{-1}). The cumulative ˙OH production in [Fe(III) + LB]/H_2O_2 was measured to be 3.28 times that in LB/H_2O_2, while the cumulative ˙OH production in [Fe(III) + WB]/H_2O_2 was 11.9 times that in WB/H_2O_2. No extra consumption of H_2O_2 was observed in LB/H_2O_2 or WB/H_2O_2 after addition of trace Fe(III). Consequently, the reaction rate constants (k_{obs}) for oxidation of pollutants (2,4-dichlorophenoxyacetic acid and sulfamethazine) were enhanced by 3.13–9.16 times. Other iron species including dissolved Fe(II) and iron minerals showed a similar effect on catalyzing 2,4-D oxidation by biochar/H_2O_2. The interactions involved in adsorption and reduction of Fe(III) by biochar in which the defects acted as electron donors and oxygen-containing functional groups bridged the electron transfer. The fast regeneration of Fe(II) in the co-catalytic system resulted in the sustainable ˙OH production, thus the efficient oxidation of pollutants comparable to other advanced oxidation processes was achieved by using dissolved iron at a concentration as low as the concentration that can be found in natural water.

Received 14th March 2022
Accepted 5th June 2022

DOI: 10.1039/d2ra01647h

rsc.li/rsc-advances

1. Introduction

Biochar is a kind of carbon-rich material obtained by pyrolysis of waste biomass under oxygen-limited conditions, and has shown great potential in carbon sequestration, soil improvement, energy storage, and environmental remediation.[1–3] Recently, biochar has been found to be an attractive catalyst for advanced oxidation of pollutants.[4–6] Specifically, biochar can activate H_2O_2,[7–10] and persulfates[11–13] to produce reactive oxygen species (ROS) such as the hydroxyl radical (˙OH), sulfate radical ($SO_4^{\bullet-}$) and singlet oxygen ($^1O_2$), which are powerful oxidants (*e.g.* E^{θ}(˙OH/H_2O) = 2.73 V) capable of mineralization of various organic pollutants.[14–16] As biochar is readily available from waste biomass, its application in remediation of contaminated environments is advantageous over other elaborately synthesized materials in view of cost and sustainability.[17–19] However, the practical application of biochar-activated systems is limited by the low yield of ROS. For example, the cumulative yield of ˙OH was estimated to be only 0.09 mol per molar consumption of H_2O_2 in a biochar/H_2O_2 system,[20] and most of the H_2O_2 was decomposed into end-products (H_2O and O_2), as has been observed on other carbon materials.[21] The low efficiency of H_2O_2 activation by biochar leads to unsatisfactory performance on pollutant removal and excess H_2O_2 consumption. So, biochar was more often applied as a carrier of catalysts,[22–25] or after special modifications[26–28] for use in advanced oxidation processes (AOPs).

Herein, we hypothesize that the H_2O_2 activation by biochar can be enhanced by using trace dissolved iron (Fe) together. Biochar, being an electron-rich and conductive carbon material, can act as a reductant of Fe(III) for persulfate activation to enhance the degradation of organic pollutants,[29,30] and can also accelerate Fe(III)/Fe(II) cycle that is the rate-limiting step in Fenton and Fenton-like processes.[31,32] Thereby, the required dosage of Fe(II) in Fenton process can be diminished substantially by biochar,[20] which is beneficial for minimizing the production of iron sludge that is still a challenge in Fenton process.[33,34] In this context, it is interesting to reduce further the iron concentration to a trace level that is close to natural environment, and to explore the interactions between trace iron and biochar on co-catalyzing the oxidation of pollutant by H_2O_2. The

[a]*College of Chemistry and Chemical Engineering, Shaoxing University, Shaoxing, Zhejiang, 312000, China. E-mail: ljf@usx.edu.cn*

[b]*College of Life Science, Shaoxing University, Shaoxing, Zhejiang, 312000, China. E-mail: jianxinshou@usx.edu.cn*

† Electronic supplementary information (ESI) available. See https://doi.org/10.1039/d2ra01647h

trace dissolved iron is ubiquitous in natural water. For example, a maximum dissolved iron of 0.163 mg L^{-1} in surface water has been reported by Nagai *et al.*,[35] and a dissolved iron of 0.295 mg L^{-1} in groundwater was reported by Gutierrez-Zapata *et al.*[36] The dissolved iron may also co-exist with organic pollutants in wastewater, especially in wastewater pretreated with iron-containing flocculants.[37] Therefore, the in-depth investigation on the co-catalysis of trace dissolved iron with biochar in oxidation process is of significance for both remediation of contaminated environment and advanced treatment of wastewater.

In this study, trace dissolved Fe(III) was used together with biochar to activate H_2O_2 for enhanced oxidation of organic pollutants. The typical Fe(III) concentration was set at 0.30 mg L^{-1}, equal to the limit of iron concentration in drinking water recommended by the World Health Organization (WHO), and close to that found in a natural water.[36] A common herbicide 2,4-dichlorophenoxyacetic acid (2,4-D) and a common antibiotic sulfamethazine (SMZ) were used for evaluating the performance of this novel oxidation process co-catalyzed by trace Fe(III) and biochar. Both 2,4-D and SMZ are popular model pollutants that have been frequently used in evaluating various AOPs, and their degradation pathways have been clarified in many previous studies.[34,38,39] Herein, we focus on the co-catalytic effect between trace dissolved Fe(III) and biochar in oxidation process, and the role of dissolved Fe(III) was highlighted by using two biochars obtained by pyrolysis of different feedstock. We will show that co-catalysis of trace Fe(III) with biochar can raise dramatically the $^{\cdot}OH$ yield from H_2O_2 decomposition, and enhance the oxidation of pollutants consequently. The interfacial interactions between trace Fe(III) and biochar in the co-catalytic system will be investigated, so as to clarify the in-depth mechanisms. Furthermore, different iron species including dissolved Fe(II) and solid iron minerals are used instead of aqueous Fe(III), so as to extend the knowledge about the applicability of this co-catalytic system in remediation of contaminated environment.

2. Experimental

2.1. Reagents and biochar samples

Ferric sulfate [$Fe_2(SO_4)_3$] and ferrous sulfate heptahydrate ($FeSO_4 \cdot 7H_2O$) of analytical grade used for preparing the solution of trace Fe(III)/Fe(II), as well as aqueous solution of H_2O_2 (30%, w/w) of analytical grade were purchased from the Sinopharm Chemical Reagent Co. Ltd., China. Benzoic acid (BA) and other chemicals (*e.g.* acetonitrile, methanol, sodium hydroxide) of analytical grade, iron minerals including hematite (Fe_2O_3, 99% purity) and magnetite (Fe_3O_4, 99% purity), and the model pollutants including 2,4-D (98% purity) and SMZ (99% purity) were purchased from Aladdin Agents Co. Ltd., China. The 18.2 MΩ cm (Milli-Q Gradient, Millipore, USA) pure water was used for preparing the solutions.

The biochar samples were derived from two different feedstock: one labeled as LB from a cereal waste after making liquor, and another labeled as WB from a pinewood sawdust, according to the method reported in our previous study.[20] The temperature of 700 °C for pyrolysis was selected for producing the biochar that has both relatively stable properties[40,41] and high reactivity in catalyzing Fenton process.[20] The carbon contents, ash contents and surface areas (Brunauer–Emmet–Teller (BET) method) were 66.0% ± 0.3% and 93.9% ± 0.4%, 23.4% ± 0.1% and 0.89% ± 0.03%, and 6.66 and 409 $m^2\ g^{-1}$, respectively for LB and WB. More details regarding the compositions of these two biochars are provided in the ESI (Table S1 and Fig. S1†). A Fourier transform infrared spectrometer (FTIR) (Nexus, Nicolet, USA) was used to identify the functional groups of biochar with KBr as the background. Raman measurements were performed using a Renishaw inVia Raman spectrometer (UK) to evaluate the defects and graphitization of biochar. An X-ray diffractometer (XRD) (Empyrean, Panalytical, Netherlands) was used to characterize the graphite-like structure in biochar.

2.2. Experimental methods of oxidation

The oxidation experiments using trace Fe(III) in biochar/H_2O_2 system were performed in the dark in an oscillator (180 rpm) (KS4000i, IKA, Germany). In a typical co-catalytic system containing 100 mL of water solution of trace Fe(III) (0.30 mg L^{-1}), the biochar (3.0 g L^{-1}) was added, and the initial pH (pH_0) adjusted to 3.0 ± 0.1 with dilute H_2SO_4 solution. The suspension was oscillated at 25 ± 0.2 °C for 30 min of preliminary equilibration. After addition of pollutant (2,4-D or SMZ) with an initial concentration (C_0) of 20 mg L^{-1}, the pH of solution was measured and re-adjusted to 3.0 ± 0.1 if necessary. Then, the reaction was initiated immediately after addition of H_2O_2 (5.0 mmol L^{-1}). After a set reaction time interval t (2–60 min), 0.5 mL of solution was sampled and immediately mixed with methanol of the same volume. The 2,4-D or SMZ concentration (C_t, mg L^{-1}), and total organic carbon (TOC) in the mixed solution samples was analyzed after membrane filtration (0.22 μm). The mean value of triplicates was recorded for each experiment. The Fe(III)/H_2O_2 and biochar/H_2O_2 systems, together with those using biochar or H_2O_2 alone were tested for comparison. Different pH_0 (2.0–4.0), and different dosages of Fe(III) (0.10–1.00 mg L^{-1}), H_2O_2 (1.0–9.0 mmol L^{-1}) and biochar (1.0–5.0 g L^{-1}) were adjusted to investigate their influence on 2,4-D degradation. The different conditions used in this study are listed in Table S2.† In further comparison studies, the trace Fe(II) solution from dissolution of $FeSO_4 \cdot 7H_2O$, and the suspensions of two iron minerals (hematite and magnetite) were used instead of Fe(III) solution to test the feasibility of various iron species. The repetitive experiments were performed to estimate the reusability of biochar by recycling it through centrifugation (8000 rpm) and freeze-drying without further purification.

2.3. Measurement of ROS in reaction systems

The $^{\cdot}OH$ production in various reaction systems was measured by using BA as a chemical probe.[42,43] The specific procedure is same as that in the oxidation experiment, except that a BA solution with initial concentration of 5.0 mmol L^{-1} was used instead of pollutant solution. The solution sample was analyzed after

mixing with methanol and membrane filtration. The concentration of *p*-hydroxybenzoic acid (*p*-HBA) derived from BA oxidation was referred to calculate the cumulative amount of $^{\bullet}OH$. According to Tong *et al.*,[42] the production of 1.00 mmol of *p*-HBA is equivalent to the consumption of 5.87 mmol of $^{\bullet}OH$. The production $^{\bullet}OH$ and superoxide anion radical ($O_2^{\bullet-}$) in various reaction systems was also determined by electron paramagnetic resonance (EPR) spectrometry (FA-200, JEOL, Japan).[43]

2.4. Instrumental analysis of solution samples

The concentration of *p*-HBA, 2,4-D or SMZ was measured using high performance liquid chromatography (LC-20A, Shimadzu, Japan). The details for analysis of *p*-HBA and 2,4-D can be found in our previous study,[43] and SMZ was analyzed at 275 nm using an eluent composed of acetonitrile and 0.1% acetic acid (v/v = 40/60). The H_2O_2 or Fe(II) concentration was measured using UV-vis spectrophotometry (Spectrum 1920, Shanghai, China).[20] The total aqueous iron was measured by inductively coupled plasma-atomic emission spectrometry (ICP-AES) (Prodigy XP, Leeman, USA), and the TOC was determined on a total carbon analyzer (Elementar vario, German).

3. Results and discussion

3.1. Co-catalysis of trace Fe(III) with biochar in oxidation of pollutants by H_2O_2

The co-catalysis of trace dissolved Fe(III) (0.30 mg L^{-1}) with biochar in oxidation of 2,4-D by H_2O_2 can be found in Fig. 1. No apparent removal of 2,4-D was observed in Fe(III)/H_2O_2 (Fig. 1(a)), and only 41.8% and 35.7% of 2,4-D was removed respectively by LB/H_2O_2 (Fig. 1(a)) and WB/H_2O_2 (Fig. 1(b)), after 60 min of reaction. In contrast, much more 2,4-D was removed in the two systems co-catalyzed by dissolved Fe(III) and biochar, namely 89.0% in [Fe(III) + LB]/H_2O_2 and 96.5% in [Fe(III) + WB]/H_2O_2, after the same reaction time. The results indicate that trace Fe(III) enhanced the pollutant removal by biochar/H_2O_2, which is further proved by kinetic analysis. The obtained *pseudo*-first-order reaction rate constants (k_{obs}) show the much faster degradation of 2,4-D in the co-catalytic systems (Fig. 1(c)), as the k_{obs} values for 2,4-D removal in [Fe(III) + LB]/H_2O_2 and [Fe(III) + WB]/H_2O_2 are respectively 4.64 and 9.16 times that in LB/H_2O_2 and WB/H_2O_2, and are two orders of magnitude larger than that the k_{obs} value in Fe(III)/H_2O_2. The k_{obs} values (0.035–0.055 min^{-1}) in these [Fe(III) + biochar]/H_2O_2 systems are also larger than that observed in a Fenton process catalyzed by FeS[44] and in a photo-catalytic process,[45] indicating that an efficiency comparable to other AOPs can be obtained through activation of H_2O_2 using both biochar and trace Fe(III).

Additional experiments have been performed to prove that 2,4-D was removed through oxidation. First, the contribution of adsorption by biochar to the total removal is insignificant as few 2,4-D was removed by biochar itself within 60 min (LB in Fig. 1(a), and WB in Fig. 1(b)). Second, the TOC removal in the reaction systems using H_2O_2 (Fig. 1(d)) proves that 2,4-D was removed mostly by oxidation. Much more TOC was removed in [Fe(III) + WB]/H_2O_2 and [Fe(III) + LB]/H_2O_2 than that in WB/H_2O_2

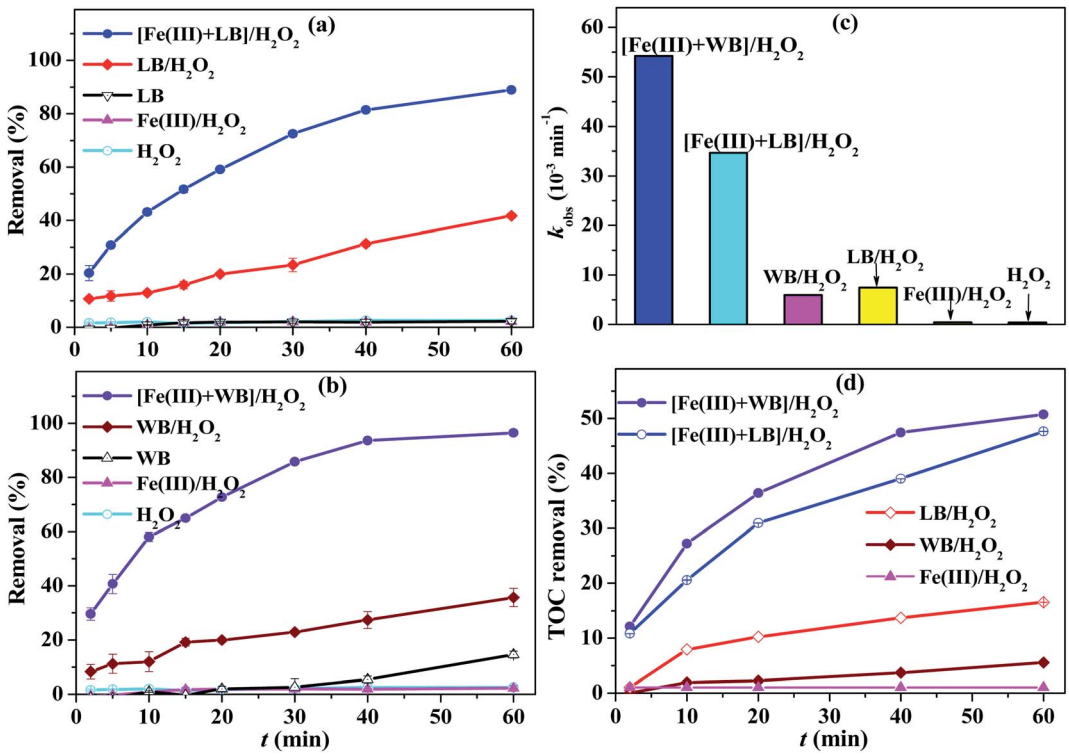

Fig. 1 (a and b) Removal of 2,4-D (C_0 = 20 mg L^{-1}) in the systems using different combinations of Fe(III), biochar (LB or WB) and/or H_2O_2; (c) k_{obs} and (d) TOC removal in different systems. Dosage: Fe(III) = 0.30 mg L^{-1}, LB or WB = 3.0 g L^{-1}, and H_2O_2 = 5.0 mmol L^{-1}; and pH_0 = 3.0.

and LB/H_2O_2, proving the enhanced mineralization of 2,4-D in both co-catalytic systems. The release of chloride ions indicates the dechlorination of 2,4-D in the reaction systems, and the much faster dechlorination was observed in [Fe(III) + WB]/H_2O_2 than in WB/H_2O_2 (Fig. S2†). The specific degradation pathway of 2,4-D in Fenton-like oxidation by H_2O_2 included dechlorination, hydroxylation, and opening of the aromatic ring, with the short-chain organic acids dominated the residual TOC.[43] Furthermore, the co-catalysis of trace Fe(III) (0.30 mg L^{-1}) with biochar was also found in oxidation of another pollutant SMZ (Fig. S3†). The removal of SMZ in [Fe(III) + LB]/H_2O_2 is much faster than in either Fe(III)/H_2O_2 or LB/H_2O_2, and the k_{obs} for SMZ removal in [Fe(III) + LB]/H_2O_2 is calculated to be 13.6×10^{-3} min^{-1}, which is 3.13 times that in LB/H_2O_2, and 6.07 times that in Fe(III)/H_2O_2. The results prove that the co-catalytic system is applicable for oxidation of different organic pollutants. It needs to be mentioned in advance here that, the difference between the two biochars (LB *vs.* WB) on performance for pollutant removal in the co-catalytic system will be addressed in the Section 3.5.

3.2. Enhanced ·OH yield in the co-catalytic system

Much more ·OH was produced in the two systems co-catalyzed by biochar and trace Fe(III) (0.30 mg L^{-1}) than that in biochar/H_2O_2, according to results shown in Fig. 2(a). The cumulative ·OH productions in [Fe(III) + WB]/H_2O_2 and [Fe(III) + LB]/H_2O_2 are respectively 11.9 and 3.28 times that in WB/H_2O_2 and LB/H_2O_2, and more than ten times that in Fe(III)/H_2O_2. The most ·OH production (1.11 mmol L^{-1}) was observed in [Fe(III) + WB]/H_2O_2 after 60 min of reaction, which can explain the highest k_{obs} and the most TOC removal in this system (Fig. 1(c) and (d)). The ranking of various reaction systems on ·OH production is generally in consistency with their order on k_{obs} values (Fig. 1(c)), namely, more ·OH production resulted in faster oxidation of pollutant. However, the ranking of H_2O_2 consumption in different systems is not always consistent with ·OH production. More decomposition of H_2O_2 was observed in the two systems using LB (Fig. 2(b)), namely [Fe(III) + LB]/H_2O_2 and LB/H_2O_2. The H_2O_2 consumed in [Fe(III) + WB]/H_2O_2 is comparable to that in WB/H_2O_2, despite that the ·OH production in [Fe(III) + WB]/H_2O_2 was the most among all the systems (Fig. 2(a)). Therefore, the activation efficiency of H_2O_2 should be estimated on the basis of ·OH yield, namely the molar production of ·OH per molar decomposition of H_2O_2. In fact, the ·OH yield in the two biochar-activated systems is fairly low (6.19% in WB/H_2O_2, and 9.27% in LB/H_2O_2), indicating that most (>90%) of H_2O_2 decomposed into end-products (H_2O and O_2).[21] In contrast, addition of trace Fe(III) in biochar/H_2O_2 enhanced dramatically the ·OH yield (89.8% in [Fe(III) + WB]/H_2O_2, and 32.5% in [Fe(III) + LB]/H_2O_2), without extra consumption of H_2O_2 (Fig. 2(b)). Therefore, biochar facilitated the decomposition of H_2O_2 while trace Fe(III) boosted the yield of ·OH in the co-catalytic systems. The similar co-catalytic effect on enhancing the ·OH yield from H_2O_2 decomposition has been observed in the combination of biochar with iron minerals,[43,46] and in the Fenton-like systems with presence of

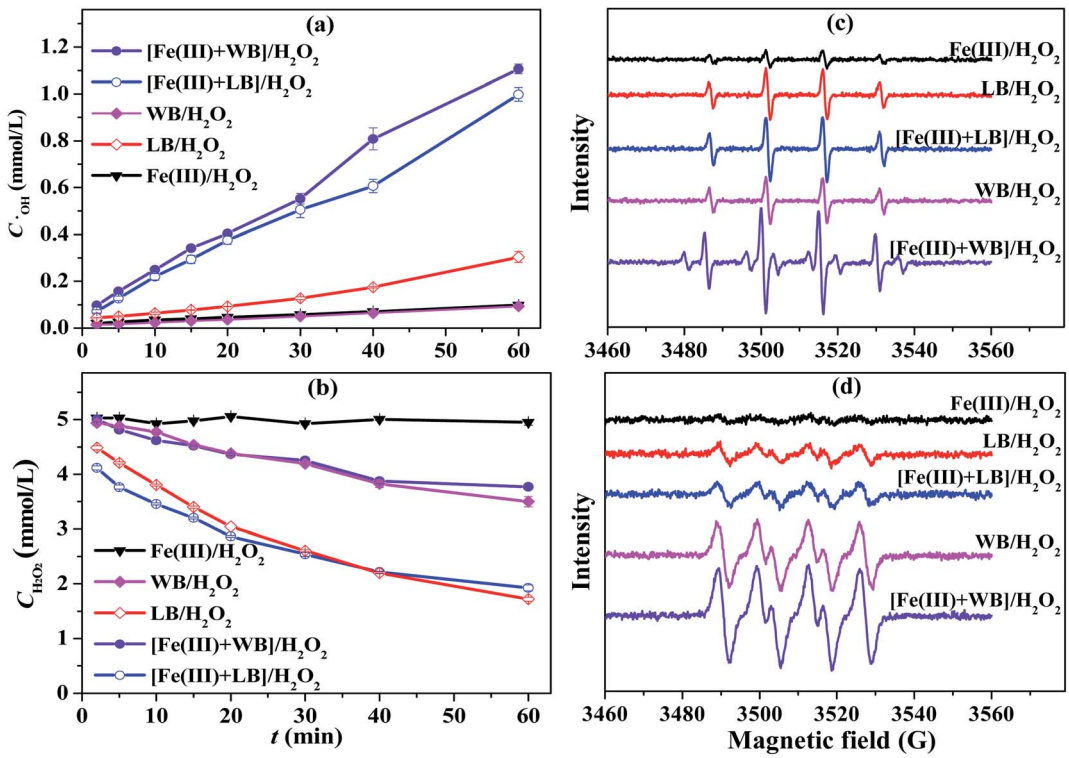

Fig. 2 (a) Cumulative ·OH production, and (b) change of H_2O_2 concentration, (c) EPR spectra of ·OH trapped by DMPO, and (d) EPR spectra of $O_2^{\cdot-}$ trapped by DMPO and methanol in different oxidation systems. Dosage: Fe(III) = 0.30 mg L^{-1}, LB or WB = 3.0 g L^{-1}, and H_2O_2 = 5.0 mmol L^{-1}; and pH_0 = 3.0.

activated carbon, carbon nanotubes and reduced graphene oxide.[47,48]

The EPR spectra confirm the production of both ·OH and $O_2^{\cdot-}$ in most of the reaction systems. The ·OH signals with characteristic 1 : 2 : 2 : 1 pattern (Fig. 2(c)) can be ranked by relative intensity in an order similar to the ·OH production shown in Fig. 2(a). Namely, the stronger ·OH signals belonging to the two co-catalytic systems are consistent with the more production of ·OH measured with chemical probe. Furthermore, the degradation experiments using methanol as the ·OH scavenger has been performed for verifying the role of ·OH. The results (Fig. S4(a)†) indicated that the degradation of 2,4-D was almost ceased when methanol was added in the reaction systems, proving that ·OH is the dominant ROS in both [Fe(III) + biochar]/H_2O_2 and biochar/H_2O_2 systems. Despite this, the signals of 1 : 1 : 1 : 1 pattern shown in Fig. 2(d) indicates that there was $O_2^{\cdot-}$ in the reaction systems except Fe(III)/H_2O_2. Chloroform ($CHCl_3$) was used as the scavenger of $O_2^{\cdot-}$ according to a previous study by Diao *et al.*[49] The experimental results indicate that $O_2^{\cdot-}$ had contributed to 2,4-D degradation as well, because addition of chloroform in [Fe(III) + LB]/H_2O_2 slowed down the 2,4-D degradation (Fig. S4(b)†). As $O_2^{\cdot-}$ is a reductant ($E^0(O_2/O_2^{\cdot-} = -0.16$ V)), it contributed to 2,4-D degradation most likely by serving as the intermediate for production of ·OH.[43,50]

3.3. Effect of Fe(III) concentration and iron species

The influence of Fe(III) concentration on production of ·OH in [Fe(III) + LB]/H_2O_2 is shown in Fig. 3(a). As can be seen, more Fe(III) resulted in production of more ·OH and subsequently faster oxidation of 2,4-D (Fig. 3(b)). Specifically, the 2,4-D degradation rate was enhanced sharply when the Fe(III) concentration increased from 0 to 0.30 mg L^{-1}. But after then, the enhancement of degradation rate was no longer so distinct. The dissolved iron may also exist in water in ferrous species (Fe(II)), especially in anaerobic environment. For this case, a comparison study using Fe(II) instead of Fe(III) was conducted to degrade 2,4-D under the same reaction conditions. The results (Fig. 3(c)) indicate that 2,4-D was degraded in [Fe(II) + LB]/H_2O_2 with a reaction rate (k_{obs}) a little higher than that in [Fe(III) + LB]/H_2O_2, but much higher than that in the Fenton process without biochar (Fe(II)/H_2O_2). Therefore, the trace iron of both valence (Fe(III) and Fe(II)) is applicable in the co-catalyzed oxidation of pollutant by H_2O_2.

Iron minerals have been used as the iron source for catalyzing the Fenton-like processes,[51,52] so we hypothesize that the solid iron species can also be used together with biochar for co-catalyzing the oxidation of pollutants by H_2O_2. In this study, two common iron minerals, namely hematite (Fe_2O_3) and magnetite (Fe_3O_4), were used together with WB for activation of H_2O_2 at pH_0 of 3.0. The results in Fig. 3(d) show the enhanced 2,4-D removal by both [Fe_2O_3 + WB]/H_2O_2 and [Fe_3O_4 + WB]/H_2O_2, with the removal efficiencies apparently higher than the simple sum of WB/H_2O_2 and corresponding heterogeneous Fenton system (Fe_2O_3/H_2O_2 or Fe_3O_4/H_2O_2). In addition, the dissolved iron was measured to be 0.073 and 0.26 mg L^{-1} after reaction in [Fe_2O_3 + WB]/H_2O_2 and [Fe_3O_4 + WB]/H_2O_2, respectively. The 2,4-D degradation rate by [Fe_3O_4 + WB]/H_2O_2 is comparable to that obtained in [Fe(III) + WB]/H_2O_2 with a dissolved Fe(III) of 0.30 mg L^{-1}, while the degradation rate by [Fe_2O_3 + WB]/H_2O_2 is close to that obtained with a dissolved Fe(III) of 0.10 mg L^{-1} (Fig. S5†). Therefore, it is likely that the iron minerals catalyzed

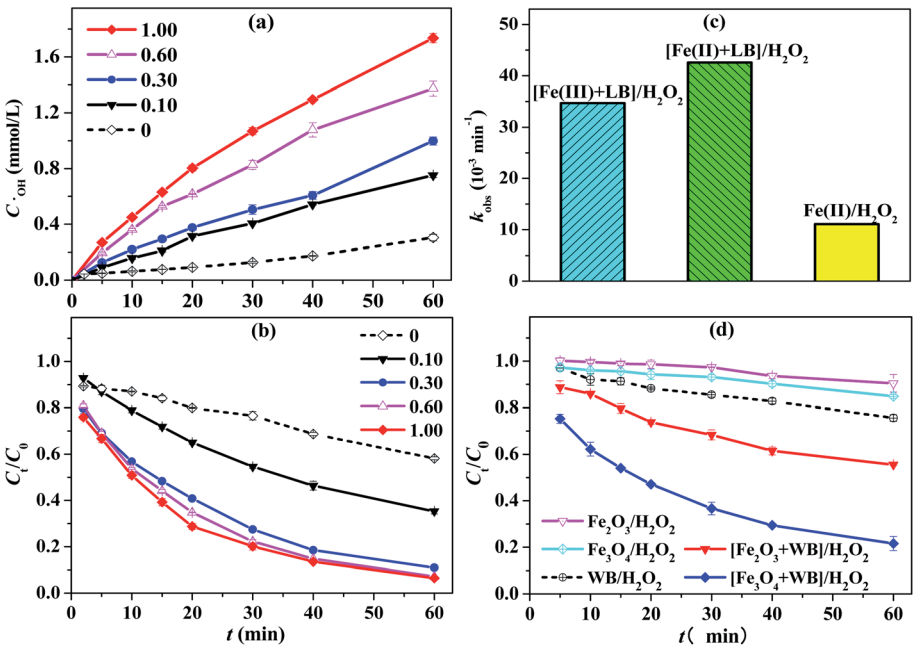

Fig. 3 (a) Cumulative ·OH production, and (b) removal of 2,4-D ($C_0 = 20$ mg L^{-1}) by [Fe(III) + LB]/H_2O_2 with different Fe(III) concentrations; (c) k_{obs} of 2,4-D removal in [Fe + LB]/H_2O_2 using Fe(II) instead of Fe(III), and (d) removal of 2,4-D ($C_0 = 20$ mg L^{-1}) in the oxidation systems using WB (1.0 g L^{-1}) and iron minerals (1.0 g L^{-1}). Dosage: LB = 3.0 g L^{-1} (if present), and H_2O_2 = 5.0 mmol L^{-1}; and pH_0 = 3.0.

the degradation of pollutants in biochar/H_2O_2 through releasing dissolved iron at acidic pH.[43,53,54] The more and in-depth investigations are underway to clarify the mechanisms involved in the activation of H_2O_2 by both biochar and iron minerals. Herein, the preliminary investigation validated the same role of dissolved iron from solid minerals on catalyzing the oxidation of pollutant in biochar/H_2O_2. These results, together with that obtained by using both Fe(III) and Fe(II) species, are significant for remediation of contaminated environment by utilizing the ubiquitous iron in water and soil. Furthermore, the co-catalysis of trace dissolved iron with biochar for activation of H_2O_2 is also advantageous for treatment of wastewater, because the production of iron sludge can be minimized at an iron concentration as low as 0.3 mg L^{-1}. For validating this, the solution after reaction in [Fe(III) + LB]/H_2O_2 was separated out and its pH was adjusted from acidic to neutral (6.5). The solution maintained to be clear after the pH adjustment (Fig. S6†), proving that the iron sludge was hardly produced.

3.4. Interactions between dissolved Fe(III) and biochar

The enhanced activation of H_2O_2 in the co-catalytic system is related to the interfacial interactions between dissolved iron and biochar, which was investigated using a Fe(III) concentration of 1.00 mg L^{-1}, because the lower concentration (*e.g.* 0.30 mg L^{-1}) makes it difficult to measure accurately the concentration of regenerated Fe(II). First, the results shown in Fig. 4 indicate that a significant fraction of aqueous Fe(III) was transformed into Fe(II) during the oxidation of 2,4-D in [Fe(III) + biochar]/H_2O_2. There was hardly any Fe(II) detected in Fe(III)/H_2O_2, while the Fe(II) concentrations in [Fe(III) + LB]/H_2O_2 and [Fe(III) + WB]/H_2O_2 reached to 0.451 and 0.608 mg L^{-1} after 60 min, respectively. Therefore, nearly 45% and 80% of aqueous iron were present in Fe(II) species in [Fe(III) + LB]/H_2O_2 and [Fe(III) + WB]/H_2O_2, respectively, if calculated on the basis of total aqueous iron measured at 60 min. Second, the total aqueous iron in [Fe(III) + WB]/H_2O_2 (~0.75 mg L^{-1}) is apparently fewer than the added Fe(III) (1.00 mg L^{-1}), and the total aqueous iron in [Fe(III) + LB]/H_2O_2 is also fewer than the sum of added Fe(III) (1.00 mg L^{-1}) and the released Fe (~0.3 mg L^{-1}) from LB. The results indicate that nearly 25% of aqueous iron was adsorbed by biochar.

The reduction and adsorption of aqueous Fe(III) by other carbon materials in the Fenton-like process have been reported previously. Qin *et al.*[55] found that Fe(III) ions were adsorbed onto the surface of hydrothermal carbon (HTC) to form complexes with hydroxyl groups. Then Fe(III) was reduced into Fe(II) through electron transfer from persistent free radicals (PFRs) in HTC with the mediation of Fe(III) complexes. Peng *et al.*[56] suggested that the reduction of Fe(III) by carbon nanotubes (CNTs) occurred through direct electron transfer or mediated by adsorption of both Fe(III) and H_2O_2 onto CNTs surface. Yang *et al.*[57] proposed a new pathway for the fast reduction of Fe(III) in a Fenton-like process with presence of functionalized multi-walled carbon nanotubes (FCNT-H), namely Fe(III) was reduced by H_2O_2 through a mediation of Fe(III) complexes with carboxyl groups on the FCNT-H surface. Like these carbon materials, biochar has shown its potential in electron donation and transfer in AOPs, but the specific routes are different for the biochars prepared at different conditions. For example, Wang *et al.*[29] and Hong *et al.*[34] have proposed that PFRs in the biochar prepared at 500 °C were the dominant electron donors to reduce Fe(III) for activation of persulfates. However, our previous study has shown that the biochar prepared at 700 °C was more reactive on facilitating the Fe(III)/Fe(II) cycle in Fenton process,[20] although Yang *et al.*[58] and Zeng *et al.*[30] have reported that there are few PFRs in the biochar prepared at 700 °C. Therefore, PFRs are not likely to be the major electron donors for reduction of Fe(III) in this study. Recently, Ouyang *et al.*,[59] and Wang and Chen[60] proposed that the defects in the biochar prepared at high temperature (700–900 °C) acted as electron donors for activation of persulfates. In addition, the graphite-like structure in biochar facilitated the electron transfer.[61–63] In the two biochars (LB and WB) used in this study, the defects was proved by the relatively high intensity ratios of D-band (1350 cm^{-1}) to G-band (1570 cm^{-1}) (I_D/I_G) in Raman spectra (Fig. 5(a)), and the graphite-like structure was confirmed by the two bands at 2θ = 23.5 and 43.5° in XRD patterns (Fig. 5(b)). So, it can be supposed

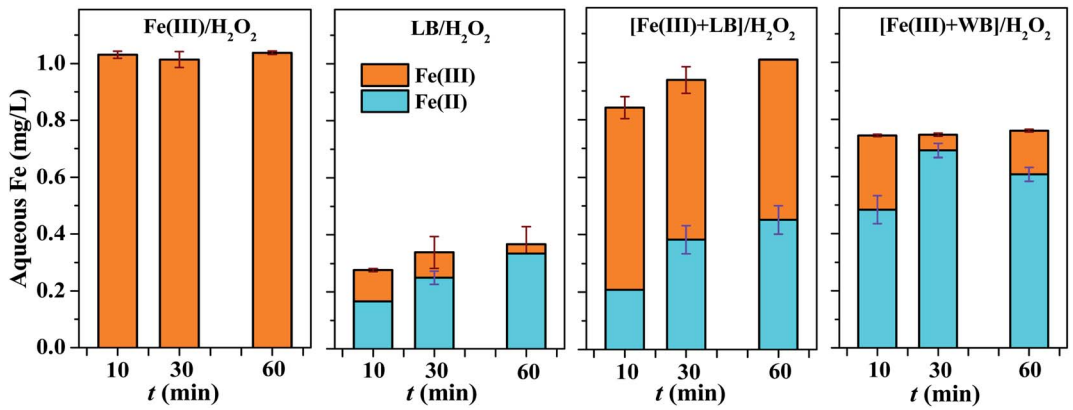

Fig. 4 Change of total Fe and Fe(II) concentrations in the solutions of different oxidation systems. Dosage: Fe(III) = 1.00 mg L^{-1}, LB or WB = 3.0 g L^{-1}, and H_2O_2 = 5.0 mmol L^{-1}; and pH_0 = 3.0.

that the defects and graphite-like structure in LB and WB contributed to the electron donation/transfer for direct reduction of Fe(III) by biochar. Such direct reduction is further proved by mixing biochar in aqueous Fe(III) solution (Fig. 5(d)). As expected, Fe(II) accounted for 73% and 84% (at 60 min) of aqueous iron in the suspension of Fe(III) + LB and Fe(III) + WB, respectively. Furthermore, the surface hydroxyl groups were observed by FTIR in both biochars (Fig. 5(c)), and carboxyl groups were found in the biochars recycled after reaction (Fig. S7†). These oxygen-containing functional groups can form complexes with Fe(III),[55,57] which bridged the electron transfer from biochar to reduce Fe(III). Thus, the reduction of Fe(III) by biochar makes the regeneration of Fe(II) fast enough for catalyzing the sustainable $^{\cdot}OH$ production (eqn (1) and (2)), so that the efficient oxidation of pollutant was achieved even at a trace level of iron supply in the co-catalytic system. However, the trace iron used in this study makes it difficult to obtain more specific information about the Fe(III) complexation on biochar.

$$Fe(II) + H_2O_2 \rightarrow Fe(III) + {}^{\cdot}OH + OH^- \quad (1)$$

$$Biochar \Rightarrow e + Fe(III) \rightarrow Fe(II) \quad (2)$$

3.5. Comparison between two biochars

The different performance on pollutant removal between the two biochars, LB and WB, was observed in different oxidation systems. First, the faster degradation of 2,4-D was observed in LB/H_2O_2 than that in WB/H_2O_2 (both without added Fe(III)) (Fig. 1(c)), despite the higher adsorption of 2,4-D by WB than that by LB, according to the adsorption isotherms obtained after 24 h of equilibration (Fig. S8†). The faster 2,4-D degradation in LB/H_2O_2 corresponds to the relatively more $^{\cdot}OH$ production in LB/H_2O_2 than that in WB/H_2O_2 (Fig. 2(a)). The results indicate the relatively higher reactivity of LB for activation of H_2O_2, which should be ascribed to the different compositions of biochar. Huang *et al.*[64] and Tao *et al.*[65] have reported that the inorganic components such as metals in biochar contributed significantly to activation of H_2O_2. In this study, there are more inorganic components in LB than in WB, as indicated by the higher ash content (23.4% *vs.* 0.89%) and lower carbon content (66.0% *vs.* 93.9%) in LB (Table S1†). The iron leaching was observed in LB/H_2O_2 (Fig. 4), indicating there are trace protogenetic iron species in LB. Besides, nitrogen element (3.36% by weight) derived from the biomass feedstock was detected in LB, indicating some pyrogenic N species in LB. Both Fe and N species inherent in biochar have been reported to be favorable for enhancing the activation of peroxides.[26,64] Despite this, the yield of $^{\cdot}OH$ in LB/H_2O_2 is still very low (9.27%) when calculated on the basis of much consumption of H_2O_2 (Fig. 2(b)). So, there should be some components in LB that impeded the transformation of H_2O_2 into $^{\cdot}OH$, except those favored the production of $^{\cdot}OH$.

Different from that observed in biochar/H_2O_2, the higher k_{obs} for oxidation of 2,4-D and more TOC removal were obtained in

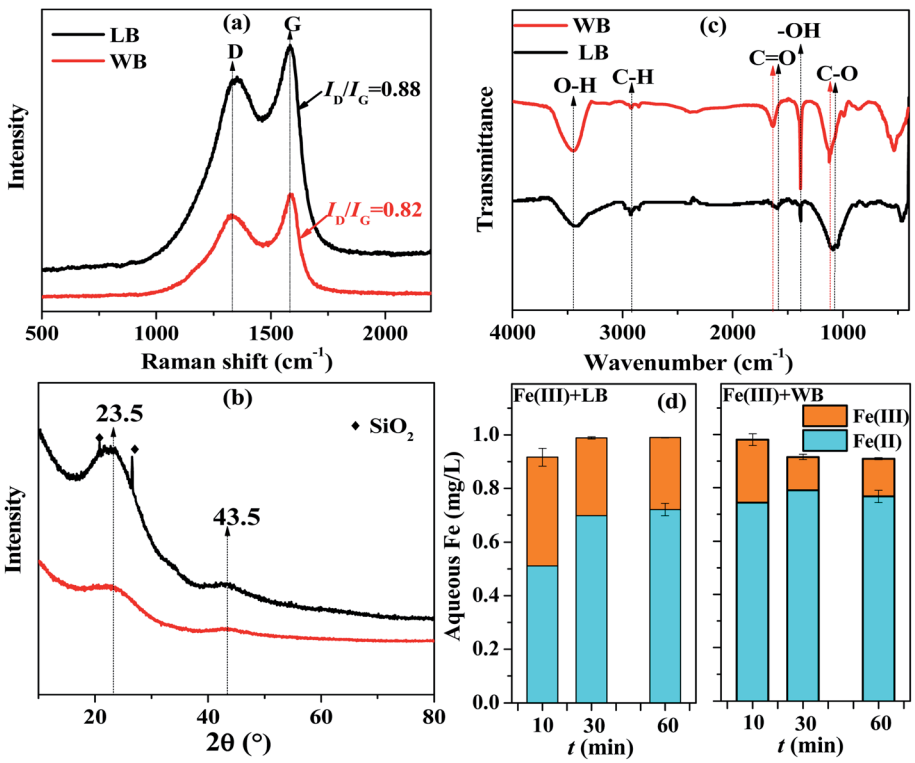

Fig. 5 (a) Raman spectra, (b) XRD patterns, and (c) FTIR of LB and WB samples; and (d) change of total Fe and Fe(II) concentrations in the mixtures of biochar (3.0 g L^{-1}) and Fe(III) solution (1.00 mg L^{-1}) at $pH_0 = 3.0$.

[Fe(III) + WB]/H_2O_2 than those in [Fe(III) + LB]/H_2O_2 (Fig. 1(c) and (d)), which is in consistency with the more $^{\bullet}OH$ production in the former system (Fig. 2(a)). Furthermore, the apparently higher $^{\bullet}OH$ yield in [Fe(III) + WB]/H_2O_2 (89.8%) was obtained, accompanying with apparently less consumption of H_2O_2 than in [Fe(III) + LB]/H_2O_2 (Fig. 2(b)). As there is hardly any inorganic component in WB, the enhanced $^{\bullet}OH$ yield should be derived from the interfacial interactions between biochar and the added trace Fe(III). Fig. 4 shows that the aqueous Fe(II) concentration in [Fe(III) + WB]/H_2O_2 is apparently higher than that in [Fe(III) + LB]/H_2O_2, namely more regenerated Fe(II) in the former system. So, the performance of the co-catalytic system on pollutant removal relies heavily on regeneration of Fe(II), as Fe(II) is much more efficient on catalyzing the production of $^{\bullet}OH$ than biochar. The relatively purer carbon matrix of WB, as indicated by its higher carbon content (93.9%), makes it a better conductor for electron transfer to reduce Fe(III). The high surface area of WB also favors electron transfer to Fe(III) by providing more reactive sites. Besides the direct reduction of Fe(III) by biochar, another possible route (eqn (3) and (4)) involving $O_2^{\bullet-}$ should also contribute to the regeneration of Fe(II) in [Fe(III) + WB]/H_2O_2, because more $O_2^{\bullet-}$ was produced in [Fe(III) + WB]/H_2O_2 than that in [Fe(III) + LB]/H_2O_2 according to the EPR analysis (Fig. 2(d)). $O_2^{\bullet-}$ was produced from electron transfer from biochar to O_2, the byproduct of H_2O_2 decomposition, according to that reported by Fang *et al.*[66] Therefore, the direct and indirect reduction of Fe(III) by biochar dominated the performance of the co-catalytic system on pollutant removal, and the specific routes of electron transfer from biochar (the electron donor) involved in adsorption of Fe(III) by biochar and mediation of H_2O_2/O_2.

$$O_2^{\bullet-} + H^+ \rightleftharpoons HO_2^{\bullet} \quad (3)$$

$$Fe(III) + HO_2^{\bullet} \rightarrow Fe(II) + O_2 + H^+ \quad (4)$$

3.6. Effect of other reaction conditions and reusability of biochar

The [Fe(III) + LB]/H_2O_2 system was chosen for further investigations on the influence of other reaction conditions including pH_0, biochar and H_2O_2 dosages on the degradation rate of 2,4-D. One reason is that LB derives from the liquor waste that is seldom utilized, and another reason is related to its poor adsorption to 2,4-D, which is favorable for highlighting the contribution of oxidation to 2,4-D removal. First, pH is the most influential factor determining the oxidation efficiency of organic pollutants in AOPs. In this study, the faster degradation of 2,4-D was recorded at pH_0 = 2.5–3.0 in [Fe(III) + LB]/H_2O_2 (Fig. 6(a)), which is same as that observed in ordinary Fenton process. pH monitoring during the reaction indicates that there was not apparent fluctuation from the initial pH_0, except at pH_0 = 4.0 when the degradation was very slow (Fig. S9†). The stable pH during reaction implies that the release of OH^- along with $^{\bullet}OH$ production (eqn (1)) was neutralized by release of H^+ from interactions between Fe(III) and biochar, such as complexation of Fe(III) with hydroxyl and carboxyl groups in biochar. The pH higher than 4.0 leads to the precipitation of Fe(III) hydroxides, so that the regeneration of Fe(II) will be suppressed. In contrast, the excess acidity may suppress the formation of Fe(III)

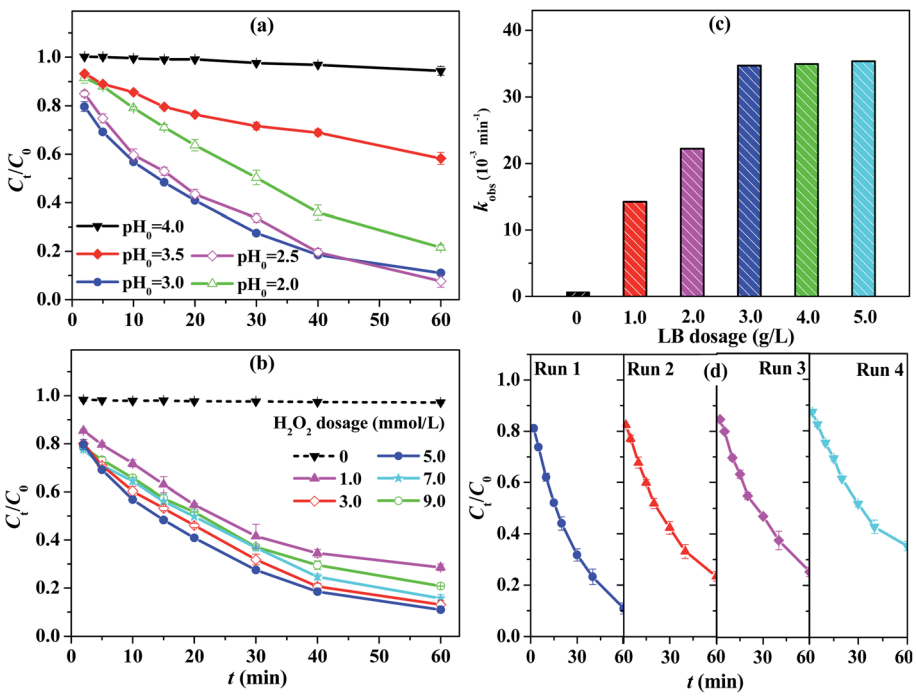

Fig. 6 Removal of 2,4-D (C_0 = 20 mg L^{-1}) at (a) different pH_0, and (b) different H_2O_2 dosage; (c) Change of k_{obs} with LB dosage; and (d) 2,4-D removal in [Fe(III) + LB]/H_2O_2 with repetitive use of LB. Typical conditions (except the variable): Fe(III) = 0.30 mg L^{-1}, LB = 3.0 g L^{-1}, and H_2O_2 = 5.0 mmol L^{-1}; and pH_0 = 3.0.

complexes, which is not favorable for regeneration of Fe(II) either. Overall, the performance of the co-catalytic system on oxidation of pollutant still relies heavily on acidic pH, which needs improvement with additional measures in future work. For example, using natural chelating reagents may enhance the efficiency of oxidative removal of organic pollutants at neutral pH.[67] Second, the degradation reaction in [Fe(III) + LB]/H_2O_2 is not as sensitive to H_2O_2 dosage as to pH (Fig. 6(b)). The 2,4-D degradation remained at a relatively fast rate when the H_2O_2 dosage was as low as 1.0 mmol L^{-1}, although the fastest one was observed at 5.0 mmol L^{-1}. Less H_2O_2 dosage led to insufficient supply of H_2O_2 and slowed down the degradation at latter reaction stage, while oversupply of H_2O_2 also resulted in slower pollutant degradation due to its reaction with $^{\bullet}OH$.[68] In this study, the high $^{\bullet}OH$ yield from H_2O_2 decomposition reduced the H_2O_2 dosage required in the co-catalytic system, which is beneficial for reducing the cost in water treatment. Third, the degradation rate of 2,4-D in [Fe(III) + LB]/H_2O_2 became faster with the increase of LB dosage from 1.0 to 3.0 g L^{-1} (Fig. 6(c) and Fig. S10†). The k_{obs} was enhanced from 14.2×10^{-3} to 34.7×10^{-3} min^{-1}, and the removal efficiency was lifted from 63.3% to 89.0% after 60 min of reaction. The biochar of higher dosage can provide more reactive sites for regeneration of Fe(II), which leads to the faster oxidation of pollutants. However, further increase of biochar dosage above 3.0 g L^{-1} did not lead to significant change on the degradation rate of 2,4-D. The reason should be due to the trace amount of Fe(III) used in this study, which limited the total amount of regenerated Fe(II).

Finally, the reusability of biochar in the co-catalytic system for removal of 2,4-D was evaluated. As can be seen in Fig. 6(d), the oxidation of 2,4-D in [Fe(III) + LB]/H_2O_2 gradually slowed down after each sequential run. The declining reactivity of biochar in repetitive experiments is supposed to be resulted from surface contamination by the intermediates (such as short-chain organic acids) derived from incomplete 2,4-D degradation, because the biochar was reused directly without any purification. Another reason may be related to the surface oxidation of biochar.[69] The more carboxyl groups were observed by FTIR (Fig. S7†) on the recycled biochar, confirming the change of surface properties of biochar after reaction. The decrease of biochar's surface area after reaction (*e.g.* from 409 m^2 g^{-1} to 360 m^2 g^{-1} for WB) implies fewer reactive sites available for repetitive use. However, no other apparent change can be found by XRD analysis (Fig. S11†) and SEM observation (Fig. S12†) of the recycled biochar, indicating there is not structural change occurred on biochar during the reaction. Further extension of reaction time may help transform the degradation intermediates more completely and enhance the reusability of biochar. For example, 2,4-D was removed completely by [Fe(III) + LB]/H_2O_2 after 180 min of reaction, accompanied with an enhanced TOC removal to 71.2%.

4. Conclusions

The co-catalysis of trace dissolved Fe(III) with biochar significantly enhanced the activation of H_2O_2, and consequently accelerated the oxidation of organic pollutants with a reaction rate comparable to other AOPs. Replacement of dissolved Fe(III) with aqueous Fe(II) and iron minerals (hematite and magnetite) also showed the similar catalytic effect on pollutant degradation by biochar/H_2O_2. The interfacial interactions between dissolved Fe(III) and biochar resulted in fast regeneration of Fe(II) in the co-catalytic system. The defects in biochar acted as the major electron donors, and the graphite-like structure and oxygen-containing functional groups in biochar facilitated the electron transfer. The aqueous iron at trace level (0.3 mg L^{-1}) prevented the precipitation of iron sludge, and biochar is advantageous over other elaborately synthesized materials in view of cost and sustainability, so their cooperation provides an efficient way to enhance the performance of AOPs on wastewater treatment. Furthermore, as dissolved iron can be found in natural water, its potential on enhancing the activation of H_2O_2 by biochar may be utilized for remediation of contaminated environment. The future work should address the influence of co-solutes in water on performance of this novel co-catalytic oxidation system, and its applicability at neutral pH should be improved with additional measures.

Author contributions

Dongqing Feng: methodology, investigation, writing – original draft. Jianxin Shou: conceptualization, investigation, writing – review & editing, funding acquisition. Sen Guo: investigation. Mengna Ya: validation. Jianfa Li: methodology, investigation, writing – review & editing, funding acquisition. Huaping Dong: investigation, funding acquisition. Yimin Li: supervision.

Conflicts of interest

The authors declare that they have no known competing financial interests or personal relationships that could have appeared to influence the work reported in this paper.

Acknowledgements

This work was kindly supported by National Natural Science Foundation of China (No. 21777103 and 21677101), and Natural Science Foundation of Zhejiang Province of China (LY16B070004).

References

1 X. Zhu, B. Chen, L. Zhu and B. Xing, Effects and mechanisms of biochar-microbe interactions in soil improvement and pollution remediation: A review, *Environ. Pollut.*, 2017, **227**, 98–115.
2 W.-J. Liu, H. Jiang and H.-Q. Yu, Emerging applications of biochar-based materials for energy storage and conversion, *Energy Environ. Sci.*, 2019, **12**, 1751–1779.
3 B. T. Son, N. V. Long and N. T. N. Hang, The development of biomass-derived carbon-based photocatalysts for the visible-light-driven photodegradation of pollutants: a comprehensive review, *RSC Adv.*, 2021, **11**, 30574–30596.

4 Z. Wan, Y. Sun, D. C. W. Tsang, D. Hou, X. Cao, S. Zhang, B. Gao and Y. S. Ok, Sustainable remediation with an electroactive biochar system: mechanisms and perspectives, *Green Chem.*, 2020, **22**, 2688–2711.

5 X. He, N. Zheng, R. Hu, Z. Hu and J. C. Yu, Hydrothermal and pyrolytic conversion of biomasses into catalysts for advanced oxidation treatments, *Adv. Funct. Mater.*, 2021, **31**, 2006505.

6 Y. Rangraza and M. M. Heravi, Recent advances in metal-free heteroatom-doped carbon heterogonous catalysts, *RSC Adv.*, 2021, **11**, 23725–23778.

7 G. Fang, J. Gao, C. Liu, D. D. Dionysiou, Y. Wang and D. Zhou, Key role of persistent free radicals in hydrogen peroxide activation by biochar: Implications to organic contaminant degradation, *Environ. Sci. Technol.*, 2014, **48**, 1902–1910.

8 K. Luo, Q. Yang, Y. Pang, D. Wang, X. Li, M. Lei and Q. Huang, Unveiling the mechanism of biochar-activated hydrogen peroxide on the degradation of ciprofloxacin, *Chem. Eng. J.*, 2019, **374**, 520–530.

9 Y. Wang, H. Dong, L. Li, R. Tian, J. Chen, Q. Ning, B. Wang, L. Tang and G. Zeng, Influence of feedstocks and modification methods on biochar's capacity to activate hydrogen peroxide for tetracycline removal, *Bioresour. Technol.*, 2019, **291**, 121840.

10 Y. Chen, R. Wang, X. Duan, S. Wang, N. Ren and S. H. Ho, Production, properties, and catalytic applications of sludge derived biochar for environmental remediation, *Water Res.*, 2020, **187**, 116390.

11 J. Wang, Z. Liao, J. Ifthikar, L. Shi, Z. Chen and Z. Chen, One-step preparation and application of magnetic sludge-derived biochar on acid orange 7 removal *via* both adsorption and persulfate based oxidation, *RSC Adv.*, 2017, **7**, 18696–18706.

12 H. Meng, C. Nie, W. Li, X. Duan, B. Lai, Z. Ao, S. Wang and T. An, Insight into the effect of lignocellulosic biomass source on the performance of biochar as persulfate activator for aqueous organic pollutants remediation: Epicarp and mesocarp of citrus peels as examples, *J. Hazard. Mater.*, 2020, **399**, 123043.

13 Q. Wang, Y. Shi, S. Lv, Y. Liang and P. Xiao, Peroxymonosulfate activation by tea residue biochar loaded with Fe_3O_4 for the degradation of tetracycline hydrochloride: performance and reaction mechanism, *RSC Adv.*, 2021, **11**, 18525–18538.

14 R. Luo, C. Wang, Y. Yao, J. Qi and J. Li, Insights into the relationship of reactive oxygen species and anions in persulfate-based advanced oxidation processes for saline organic wastewater treatment, *Environ. Sci.: Water Res. Technol.*, 2022, **8**, 465–483.

15 X.-Y. Pei, H.-Y. Ren, D.-F. Xing, G.-J. Xie, G.-L. Cao, J. Meng, N.-Q. Ren and B.-F. Liu, Electron transfer mechanism of peroxydisulfate activation by sewage sludge-derived biochar for enhanced degradation of sulfamethoxazole, *Environ. Sci.: Water Res. Technol.*, 2021, **7**, 1563–1575.

16 J. Zhang, X. Jin, H. Zhao and C. Yang, Synergistic advanced oxidation process for enhanced degradation of organic pollutants in spent sulfuric acid over recoverable apricot shell-derived biochar catalyst, *RSC Adv.*, 2022, **12**, 1904–1913.

17 B.-C. Huang, J. Jiang, G.-X. Huang and H.-Q. Yu, Sludge biochar-based catalysts for improved pollutant degradation by activating peroxymonosulfate, *J. Mater. Chem. A*, 2018, **6**, 8978–8985.

18 P. Zhang, D. O'Connor, Y. Wang, L. Jiang, T. Xia, L. Wang, D. C. W. Tsang, Y. S. Ok and D. Hou, A green biochar/iron oxide composite for methylene blue removal, *J. Hazard. Mater.*, 2020, **384**, 121286.

19 P. V. Nidheesh, A. Gopinath, N. Ranjith, A. P. Akre, V. Sreedharan and M. Suresh Kumar, Potential role of biochar in advanced oxidation processes: A sustainable approach, *Chem. Eng. J.*, 2021, **405**, 126582.

20 D. Feng, J. Lü, S. Guo and J. Li, Biochar enhanced the degradation of organic pollutants through a Fenton process using trace aqueous iron, *J. Environ. Chem. Eng.*, 2021, **9**, 104677.

21 R. S. Ribeiro, A. M. T. Silva, J. L. Figueiredo, J. L. Faria and H. T. Gomes, The influence of structure and surface chemistry of carbon materials on the decomposition of hydrogen peroxide, *Carbon*, 2013, **62**, 97–108.

22 A. Tiya-Djowe, M.-A. Dourges, J.-L. Bruneel and H. Deleuze, Plasma-deposition of α-FeOOH particles on biochar using a gliding arc discharge in humid air: a green and sustainable route for producing oxidation catalysts, *RSC Adv.*, 2019, **9**, 4797–4805.

23 Z. Li, Y. Sun, Y. Yang, Y. Han, T. Wang, J. Chen and D. C. W. Tsang, Biochar-supported nanoscale zero-valent iron as an efficient catalyst for organic degradation in groundwater, *J. Hazard. Mater.*, 2020, **383**, 121240.

24 Y.-N. Zang, S.-S. Yang, J. Ding, S.-Y. Zhao, C.-X. Chen, L. He and N.-Q. Ren, A biochar-promoted V_2O_5/g-C_3N_4 Z-Scheme heterostructure for enhanced simulated solar light-driven photocatalytic activity, *RSC Adv.*, 2021, **11**, 15106–15117.

25 L. Li, Y. Zhang, S. Yang, S. Zhang, Q. Xu, P. Chen, Y. Du and Y. Xing, Cobalt-loaded cherry core biochar composite as an effective heterogeneous persulfate catalyst for bisphenol A degradation, *RSC Adv.*, 2022, **12**, 7284–7294.

26 S. H. Ho, Y. Chen, R. Li, C. Zhang, Y. Ge, G. Cao, M. Ma, X. Duan, S. Wang and N. Ren, N-doped graphitic biochars from C-phycocyanin extracted Spirulina residue for catalytic persulfate activation toward nonradical disinfection and organic oxidation, *Water Res.*, 2019, **159**, 77–86.

27 H. Wang, W. Guo, R. Yin, J. Du, Q. Wu, H. Luo, B. Liu, F. Sseguya and N. Ren, Biochar-induced Fe(III) reduction for persulfate activation in sulfamethoxazole degradation: Insight into the electron transfer, radical oxidation and degradation pathways, *Chem. Eng. J.*, 2019, **362**, 561–569.

28 Z. Wan, Y. Sun, D. C. W. Tsang, E. Khan, A. C. K. Yip, Y. H. Ng, J. Rinklebe and Y. S. Ok, Customised fabrication of nitrogen-doped biochar for environmental and energy applications, *Chem. Eng. J.*, 2020, **401**, 126136.

29 K. Xie, R. Han, P. Sun, H. Wang, Y. Fang, Z. Zhai, D. Ma and H. Liu, Rice husk biochar modified-$CuCo_2O_4$ as an efficient peroxymonosulfate activator for non-radical degradation of

organic pollutants from aqueous environment, *RSC Adv.*, 2021, **11**, 39467–39475.

30 L. Zeng, Q. Chen, Y. Tan, P. Lan, D. Zhou, M. Wu, N. Liang, B. Pan and B. Xing, Dual roles of biochar redox property in mediating 2,4-dichlorophenol degradation in the presence of Fe^{3+} and persulfate, *Chemosphere*, 2021, **279**, 130456.

31 X.-C. Liu, C.-S. He, Z.-Y. Shen, W.-Q. Li, N. Chen, J.-S. Song, X.-G. Zhou and Y. Mu, Mechanistic study of Fe(III) chelate reduction in a neutral electro-Fenton process, *Appl. Catal., B*, 2020, **278**, 119347.

32 H. Zhou, H. Zhang, Y. He, B. Huang, C. Zhou, G. Yao and B. Lai, Critical review of reductant-enhanced peroxide activation processes: Trade-off between accelerated Fe^{3+}/Fe^{2+} cycle and quenching reactions, *Appl. Catal., B*, 2021, **286**, 119900.

33 A. Serra-Clusellas, L. De Angelis, C. H. Lin, P. Vo, M. Bayati, L. Sumner, Z. Lei, N. B. Amaral, L. M. Bertini, J. Mazza, L. R. Pizzio, J. D. Stripeikis, J. A. Rengifo-Herrera and M. M. F. de Cortalezzi, Abatement of 2,4-D by H_2O_2 solar photolysis and solar photo-Fenton-like process with minute Fe(III) concentrations, *Water Res.*, 2018, **144**, 572–580.

34 Q. Hong, C. Liu, Z. Wang, R. Li, X. Liang, Y. Wang, Y. Zhang, Z. Song, Z. Xiao, T. Cui, B. Heng, B. Xu, F. Qi and A. Ikhlaq, Electron transfer enhancing Fe(II)/Fe(III) cycle by sulfur and biochar in magnetic FeS@biochar to active peroxymonosulfate for 2,4-dichlorophenoxyacetic acid degradation, *Chem. Eng. J.*, 2021, **417**, 129238.

35 T. Nagai, A. Imai, K. Matsushige, K. Yokoi and T. Fukushima, Dissolved iron and its speciation in a shallow eutrophic lake and its inflowing rivers, *Water Res.*, 2007, **41**, 775–784.

36 H. M. Gutierrez-Zapata, K. Rojas, J. Sanabria and J. A. Rengifo-Herrera, 2,4-D abatement from groundwater samples by photo-Fenton processes at circumneutral pH using naturally iron present: Effect of inorganic ions, *Environ. Sci. Pollut. Res.*, 2017, **24**, 6213–6221.

37 K. Lal and A. Garg, Utilization of dissolved iron as catalyst during Fenton-Like oxidation of pretreated pulping effluent, *Process Saf. Environ.*, 2017, **111**, 766–774.

38 D. Huang, Y. Wang, C. Zhang, G. Zeng, C. Lai, J. Wan, L. Qin and Y. Zeng, Influence of morphological and chemical features of biochar on hydrogen peroxide activation: Implications on sulfamethazine degradation, *RSC Adv.*, 2016, **6**, 73186–73196.

39 A. Kumar, G. Sharma, M. Naushad, A. H. Al-Muhtaseb, A. Kumar, I. Hira, T. Ahamad, A. A. Ghfar and F. J. Stadler, Visible photodegradation of ibuprofen and 2,4-D in simulated waste water using sustainable metal free-hybrids based on carbon nitride and biochar, *J. Environ. Manage.*, 2019, **231**, 1164–1175.

40 T. Nie, P. Hao, Z. Zhao, W. Zhou and L. Zhu, Effect of oxidation-induced aging on the adsorption and co-adsorption of tetracycline and Cu^{2+} onto biochar, *Sci. Total Environ.*, 2019, **673**, 522–532.

41 M. He, Z. Xu, Y. Sun, P. S. Chan, I. Lui and D. C. W. Tsang, Critical impacts of pyrolysis conditions and activation methods on application-oriented production of wood waste-derived biochar, *Bioresour. Technol.*, 2021, **341**, 125811.

42 M. Tong, S. Yuan, S. Ma, M. Jin, D. Liu, D. Cheng, X. Liu, Y. Gan and Y. Wang, Production of abundant hydroxyl radicals from oxygenation of subsurface sediments, *Environ. Sci. Technol.*, 2016, **50**, 214–221.

43 X. Zhu, J. Li, B. Xie, D. Feng and Y. Li, Accelerating effects of biochar for pyrite-catalyzed Fenton-like oxidation of herbicide 2,4-D, *Chem. Eng. J.*, 2020, **391**, 123605.

44 H. Chen, Z. Zhang, Z. Yang, Q. Yang, B. Li and Z. Bai, Heterogeneous Fenton-like catalytic degradation of 2,4-dichlorophenoxyacetic acid in water with FeS, *Chem. Eng. J.*, 2015, **273**, 481–489.

45 H. Lee, S. H. Park, Y. K. Park, S. J. Kim, S. G. Seo, S. J. Ki and S. C. Jung, Photocatalytic reactions of 2,4-dichlorophenoxyacetic acid using a microwave-assisted photocatalysis system, *Chem. Eng. J.*, 2015, **278**, 259–264.

46 G. Liu, Y. Zhang, H. Yu, R. Jin and J. Zhou, Acceleration of goethite-catalyzed Fenton-like oxidation of ofloxacin by biochar, *J. Hazard. Mater.*, 2020, **397**, 122783.

47 J. Seo, H. J. Lee, H. Lee, H. E. Kim, J. Y. Lee, H. S. Kim and C. Lee, Enhanced production of reactive oxidants by Fenton-like reactions in the presence of carbon materials, *Chem. Eng. J.*, 2015, **273**, 502–508.

48 H. Yu, G. Liu, B. Dong, R. Jin and J. Zhou, Synergistic catalytic Fenton-like degradation of sulfanilamide by biosynthesized goethite-reduced graphene oxide composite, *J. Hazard. Mater.*, 2021, **415**, 125704.

49 Z. H. Diao, J. J. Liu, Y. X. Hu, L. J. Kong, D. Jiang and X. R. Xu, Comparative study of Rhodamine B degradation by the systems pyrite/H_2O_2 and pyrite/persulfate: Reactivity, stability, products and mechanism, *Sep. Purif. Technol.*, 2017, **184**, 374–383.

50 H. Zhou, J. Peng, J. Li, J. You, L. Lai, R. Liu, Z. Ao, G. Yao and B. Lai, Insights into the role of *in situ* and *ex situ* hydrogen peroxide for enhanced ferrate(VI) towards oxidation of organic contaminants, *Water Res.*, 2021, **203**, 117548.

51 L. Lai, Y. He, H. Zhou, B. Huang, G. Yao and B. Lai, Critical review of natural iron-based minerals used as heterogeneous catalysts in peroxide activation processes: Characteristics, applications and mechanisms, *J. Hazard. Mater.*, 2021, **416**, 125809.

52 X. Nie, G. Li, S. Li, Y. Luo, W. Luo, Q. Wan and T. An, Highly efficient adsorption and catalytic degradation of ciprofloxacin by a novel heterogeneous Fenton catalyst of hexapod-like pyrite nanosheets mineral clusters, *Appl. Catal., B*, 2022, **300**, 120734.

53 A. G. Karunanayake, C. M. Navarathna, S. R. Gunatilake, M. Crowley, R. Anderson, D. Mohan, F. Perez, C. U. Pittman Jr and T. Mlsna, Fe_3O_4 nanoparticles dispersed on douglas fir biochar for phosphate sorption, *ACS Appl. Nano Mater.*, 2019, **2**, 3467–3479.

54 B. Song, Z. Zeng, E. Almatrafi, M. Shen, W. Xiong, C. Zhou, W. Wang, G. Zeng and J. Gong, Pyrite-mediated advanced oxidation processes: Applications, mechanisms, and enhancing strategies, *Water Res.*, 2022, **211**, 118048.

55 Y. Qin, L. Zhang and T. An, Hydrothermal carbon-mediated Fenton-like reaction mechanism in the degradation of alachlor: Direct electron transfer from hydrothermal carbon to Fe(III), *ACS Appl. Mater. Interfaces*, 2017, **9**, 17115–17124.

56 J. Peng, J. Xue, J. Li, Z. Du, Z. Wang and S. Gao, Catalytic effect of low concentration carboxylated multi-walled carbon nanotubes on the oxidation of disinfectants with Cl-substituted structure by a Fenton-like system, *Chem. Eng. J.*, 2017, **321**, 325–334.

57 Z. Yang, A. Yu, C. Shan, G. Gao and B. Pan, Enhanced Fe(III)-mediated Fenton oxidation of atrazine in the presence of functionalized multi-walled carbon nanotubes, *Water Res.*, 2018, **137**, 37–46.

58 J. Yang, B. Pan, H. Li, S. Liao, D. Zhang, M. Wu and B. Xing, Degradation of *p*-Nitrophenol on biochars: Role of persistent free radicals, *Environ. Sci. Technol.*, 2016, **50**, 694–700.

59 D. Ouyang, Y. Chen, J. Yan, L. Qian, L. Han and M. Chen, Activation mechanism of peroxymonosulfate by biochar for catalytic degradation of 1,4-dioxane: Important role of biochar defect structures, *Chem. Eng. J.*, 2019, **370**, 614–624.

60 W. Wang and M. Chen, Catalytic degradation of sulfamethoxazole by peroxymonosulfate activation system composed of nitrogen-doped biochar from pomelo peel: Important roles of defects and nitrogen, and detoxification of intermediates, *J. Colloid Interface Sci.*, 2022, **613**, 57–70.

61 X. Xiao, B. Chen, Z. Chen, L. Zhu and J. L. Schnoor, Insight into multiple and multilevel structures of biochars and their potential environmental applications: A critical review, *Environ. Sci. Technol.*, 2018, **52**, 5027–5047.

62 J. He, Y. Xiao, J. Tang, H. Chen and H. Sun, Persulfate activation with sawdust biochar in aqueous solution by enhanced electron donor-transfer effect, *Sci. Total Environ.*, 2019, **690**, 768–777.

63 L. Du, W. Xu, S. Liu, X. Li, D. Huang, X. Tan and Y. Liu, Activation of persulfate by graphitized biochar for sulfamethoxazole removal: The roles of graphitic carbon structure and carbonyl group, *J. Colloid Interface Sci.*, 2020, **577**, 419–430.

64 D. Huang, H. Luo, C. Zhang, G. Zeng, C. Lai, M. Cheng, R. Wang, R. Deng, W. Xue, X. Gong, X. Guo and T. Li, Nonnegligible role of biomass types and its compositions on the formation of persistent free radicals in biochar: Insight into the influences on Fenton-like process, *Chem. Eng. J.*, 2019, **361**, 353–363.

65 S. Tao, S. Liang, Y. Chen, W. Yu, H. Hou, J. Qiu, Y. Zhu, K. Xiao, J. Hu, B. Liu, Y. Wang and J. Yang, Enhanced sludge dewaterability with sludge-derived biochar activating hydrogen peroxide: Synergism of Fe and Al elements in biochar, *Water Res.*, 2020, **182**, 115927.

66 G. Fang, C. Zhu, D. D. Dionysiou, J. Gao and D. Zhou, Mechanism of hydroxyl radical generation from biochar suspensions: Implications to diethyl phthalate degradation, *Bioresour. Technol.*, 2015, **176**, 210–217.

67 H. Ren, X. Jin, C. Li, T. Li, Y. Liu and R. Zhou, Rosmarinic acid enhanced Fe(III)-mediated Fenton oxidation removal of organic pollutants at near neutral pH, *Sci. Total Environ.*, 2020, **736**, 139528.

68 X. Yu, A. Somoza-Tornos, M. Graells and M. Pérez-Moya, An experimental approach to the optimization of the dosage of hydrogen peroxide for Fenton and photo-Fenton processes, *Sci. Total Environ.*, 2020, **743**, 140402.

69 Z. Xu, M. He, X. Xu, X. Cao and D. C. W. Tsang, Impacts of different activation processes on the carbon stability of biochar for oxidation resistance, *Bioresour. Technol.*, 2021, **338**, 125555.